第 2 屆大專院校綠色化學創意競賽成果報告書

組別: 研究組

隊伍名稱: 靜宜應化易容卉

主題: 超高效率發光電化學元件(LECs)

目錄

摘要----------1

壹、動機----------2

貳、目的----------3

參、設備及器材----------4

肆、過程或方法----------5

伍、結果----------6

一、Synthesis and Structural Characterization----------6

二、Solution Photophysics----------7

三、Electrochemical Properties and Theoretical Calculations----------9

陸、討論----------11

柒、結論----------23

捌、參考資料及其他----------23

摘要

發光電化學電池（light-emitting electrochemical cells, LECs）具有溶液加工性、低操作電壓和採用惰性陰極的優異特性，因此在顯示和固態照明應用中有著極高的應用潛力。在此研究中，我們首度結合了高效率的發光材料、載子平衡及光提取的提升來進一步優化 LECs 的元件效率。橘黃光銥金屬錯合物 **(YIr)** 作為發光電化學電池的發光材料，具有較高的立體障礙和良好的載流子平衡，因此其外部量子效率（external quantum efficiency, EQE）高達 13.6%。此外，藉由主-客體搭配系統更進一步改善載子平衡並減少自我淬滅，優化後的 EQE 提高到 16.9%。最後，我們更利用嵌入在玻璃基板和氧化銦錫 (indium tin oxide, ITO) 層之間的擴散層加強捕獲迷失在器件結構中各層的光子，使 EQE 提升至 23.7%。

關鍵字：*發光電化學元件、離子性金屬錯合物、載子平衡、主-客體系統*

動機

Organic light-emitting diodes (OLEDs) have shown great potential in display and lighting applications in recent years.[1] However, some disadvantages such as time-consuming thermal-evaporation deposition processes and employing active cathodes hinder their low-cost applications in consumer electronics. The concept of light-emitting electrochemical cell (LEC) proposed by Pei et al. in 1995[2] provides an alternative approach to simplify fabrication procedures and to improve cathode stability of organic light-emitting devices. In contrast to OLEDs, the LECs have several promising advantages, *e.g.*, solution processability, low operation voltage and compatibility with air-stable cathode metals. Such characteristics result from the working mechanism of LECs, which contain ionic salts that can separate into mobile ions under an applied bias. Accumulated ions at electrodes facilitate electrochemical doping of the emissive material and consequently reduce carrier injection barrier and reduce operation voltage. Owing to the electrochemical doping, carrier injection is insensitive to the work function of cathode metal and air-stable metals can be used as cathodes. It simplifies device encapsulation and improves device lifetime. Furthermore, the LECs are generally composed of a single emissive layer and can be simply fabricated by solution processes. Easy fabrication, low power consumption and employing air-stable cathodes render LECs suitable for low-cost consumer electronics.

Since the first demonstration of LEC, various kinds of active materials, *e.g.*, conjugated polymers,[2,3] ionic transition metal complexes (iTMCs),[4–7] small molecules,[7,8] quantum dots[7,9] and perovskite nanoparticles[7,10] have been used in LECs. Among these reported materials, iTMCs possess several superior properties in comparison with other types of materials. They have stable redox properties and the intrinsically ionic feature makes them free from incorporating additional ion-conducting materials, eliminating the risk of phase separation. Most important of all, phosphorescent iTMCs generally exhibit better electroluminescence (EL) efficiencies than other fluorescent materials. Some LECs based on efficient iTMCs have been reported to achieve comparable device efficiencies with those measured from OLEDs.[11–20] In addition to development of efficient materials, optimizing

carrier balance, *i.e.*, balancing the number of electron and hole, of LECs is critical to take full advantage of efficient emissive materials. Several device engineering techniques for improving carrier balance, *e.g.*, trapping or blocking carriers,[21–23] adjusting carrier injection,[24–27] salt incorporation,[28–31] modifying carrier transporting,[32–34] emissive-layer thickness optimization[35–37] and optimizing emission zone position[19,35,38–40] have been demonstrated to improve device efficiencies of LECs.[41] Modifying carrier balance of LEC is related to electrical management of carriers in the device. On the other hand, extraction of the light trapped in the optical structure of LEC is another feasible way to enhance device efficiency with optical approaches. For instance, significantly enhanced device efficiencies of LECs have been shown by light extraction from substrate[20,42–44] and waveguide modes.[17,18,45] Recently, high external quantum efficiency (EQE) and power efficiency up to 35% and 83 lm W^{-1} from blue LECs based on substrates with embedded diffusive layers have been reported.[20] Optical optimization for light extraction is independent of the employed emissive materials and thus is effective for all LECs, especially useful for white LECs.[46–49] However, most reported works focused on a single optimization approach, *i.e.*, employing efficient emissive material, optimizing carrier balance or maximizing light extraction, but few works on a combinational way for overall optimization have been reported.

壹、 目的

The host and guest complexes used in this study are the blue-emitting complex **BG**[57] and the yellow-emitting complex **YIr** (**Scheme 1**), respectively. In the complex **YIr**, phenylpyrazole having *n*-butyl was used as C^N ligands, and 4,7-diphenyl-1,10-phenanthroline having a longer conjugated system was used as the N^N ligand, produces the complex with a relatively smaller energy gap. The introduction of *n*-butyl group on phenylpyrazole not only improves solubility, but also prevents the stacking of complexes due to the suppressed intermolecular π-π interaction. The weak aggregation-caused quenching effect induced by the suppressed intermolecular π-π interaction further enhances

the emission. With tethering phenyl groups for steric hindrance on the ancillary ligand of complex **YIr**, the photoluminescence quantum yield (PLQY) of the emissive layer of the guest-only LEC is up to *ca.* 61%. In addition, the high EQE >13% obtained from the guest-only LEC reveals superior carrier balance of the device. To reduce self-quenching effect and to further improve carrier balance, the higher-gap host complex **BG** is employed to disperse the guest molecules. When complex **YIr** is dispersed in host films of complex **BG**, the PLQYs of the emissive layers of host-guest LECs can be enhanced to >75%. The peak EQE of the optimized host-guest LEC reaches *ca.* 17%. The analysis of the optical simulation and the EL measurements results indicates that both increased PLQY of dispersed molecules of complex **YIr** and improved carrier balance of the host-guest LEC result in enhanced device efficiency. Finally, the optimized host-guest LEC is fabricated on the substrate embedded with a diffusive transparent photoresist (TPR) layer containing scattering TiO_2 nanoparticles (NPs). With enhanced light outcoupling, the peak EQE and power efficiency of *ca.* 24% and 80 lm W^{-1}, respectively, can be achieved. These results confirm that simultaneous optimization of emissive material, carrier balance and light extraction is necessary for maximizing device efficiency of LECs.

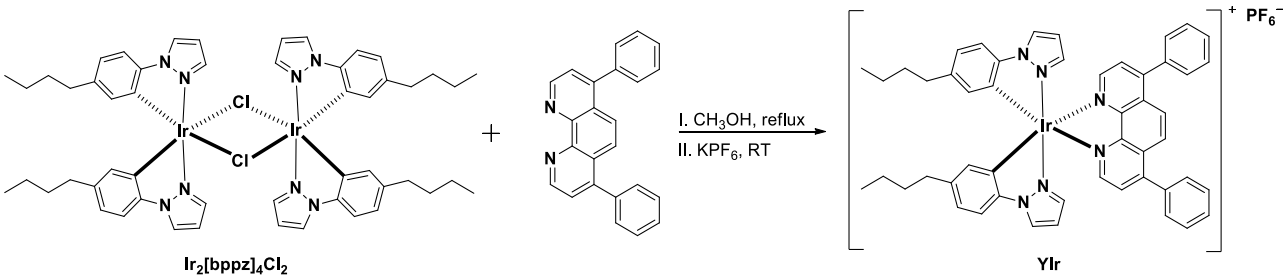

Scheme 1. Molecular structure of cationic iridium complex **YIr**.

貳、 設備及器材

^{1}H and ^{13}C NMR spectra of compounds were collected on a Bruker Ascend 400 MHz spectrometer at room temperature. Photophysical characteristics of complexes in solutions were collected at room temperature using 1×10^{-5} M acetonitrile (MeCN) solutions of all complexes on spectrofluorometer

Edinburgh FS5, which were carefully purged with nitrogen prior to measurements. UV-Vis absorption spectra were recorded on Perkin Elmer Lambda 14 spectrophotometer. Mass spectra were obtained with a THERMO Q Exactive Plus instrument operating in electrospray ionization (ESI) mode. Thermal analysis was performed by using a Mettler-Toledo, 2-HT thermogravimetric analyzer under nitrogen at a heating rate of 10℃ min^{-1}. Elemental analysis was carried out with an elementar vario EL cube elemental analyzer. To gain more insight into the electronic structure of iridium-based iTMCs, complete geometrical optimisations were performed using time-dependent density functional theory (TD-DFT) methods in solution (MeCN) with B3LYP/LANL2DZ[Ir]6-31G(d,p)[N,C,H] basis set within Gaussian 09. Oxidation and reduction potentials of all complexes were determined by cyclic voltammetry (CV) at a scan rate of 100 mV s^{-1} in MeCN solutions (1.0 mM) on ZIVE SP1. A glassy carbon electrode and a platinum wire were used as the working electrode and the counter electrode, respectively. All potentials were recorded versus the Ag/AgCl (sat'd) reference electrode. For reduction voltammograms, 0.1 M tetra-*n*-butylammonium hexafluorophosphate ($TBAPF_6$) in MeCN was used as the supporting electrolyte. Cyclometalated iridium dichlorobridged dimer, **$[Ir_2(bppz)_4Cl_2]$**, was prepared according to literature procedures.[57] All experiments involving $IrCl_3 \cdot 3H_2O$ were carried out in an inert atmosphere.

參、 過程或方法

Synthesis of complex YIr. In a round-bottomed flask, **$[Ir_2(bppz)_4Cl_2]$** (0.50 g, 0.40 mmol) and 4,7-diphenyl-1,10-phenanthroline (0.27 g, 0.80 mmol) were mixed together in 118 mL of methanol. The solution was then refluxed overnight under an inert atmosphere. After cooling to room temperature, counter ion exchange from Cl^- to PF_6^- was accomplished via a metathesis reaction in which complexes were precipitated from the methanol solution with an excess of KPF_6, washed with water and methanol, and dried under vacuum. The crude product was purified by column chromatography on silica gel (dichloromethane/acetone = 95/5) to give complex **YIr** (0.83 g, 98%) as an orange solid. ^1H NMR (400 MHz, $CDCl_3$, 298 K) δ 8.46 (d, J = 5.2 Hz, 2H), 8.13 (s, 2H), 8.07

(d, J = 2.7 Hz, 2H), 7.69 (d, J = 5.3 Hz, 2H), 7.61–7.51 (m, 10H), 7.24 (d, J = 8.1 Hz, 2H), 6.96–6.87 (m, 4H), 6.53 (t, J = 2.3 Hz, 2H), 6.23 (d, J = 1.6 Hz, 2H), 2.46 (t, J = 7.5 Hz, 4H), 1.48 (dd, J = 14.2, 7.2 Hz, 4H), 1.29–1.24 (m, 4H), 0.87 (t, J = 7.4 Hz, 6H). ^{13}C NMR (100 MHz, DMSO-d_6, 298 K) δ 150.5, 149.9, 147.6, 141.3, 140.1, 138.8, 135.6, 132.5, 132.3, 129.9, 129.6, 129.1, 128.6, 128.2, 127.0, 125.9, 122.9, 111.9, 108.2, 34.6, 32.8, 21.6, 13.7. HRMS (ESI$^+$) m/z: calcd for $C_{50}H_{46}N_6Ir^+$ [M+H]$^+$: 923.3413, found: 923.3395. Anal. calcd for $C_{50}H_{46}F_6IrN_6P$:C, 56.22; H, 4.34; N, 7.87, found C, 56.08; H, 4.43; N, 7.78.

肆、 結果

一、 Synthesis and Structural Characterization

In complex **YIr**, phenylpyrazole having *n*-butyl as an electron donating group was used as C^N ligands, and 4,7-diphenyl-1,10-phenanthroline having a longer conjugated system was used as the N^N ligand, produces the complex with a relatively smaller energy gap. The targeted complex was identified by ^{1}H NMR, ^{13}C NMR, ^{1}H-^{1}H COSY NMR, elemental analysis, and electrospray ionization-high resolution mass spectrometry (ESI-HRMS). The complex is highly soluble in DCM, CH_3CN, and DMSO, but solubility in nonpolar solvents, such as *n*-hexane and toluene, is quite limited. To further evaluate the thermal stability, complex **YIr** was subjected to thermogravimetric analysis (TGA) (**Figure 1**). The analysis showed that the decomposition temperature (T_d) was 356 ℃, indicating a high potential for electronic applications.

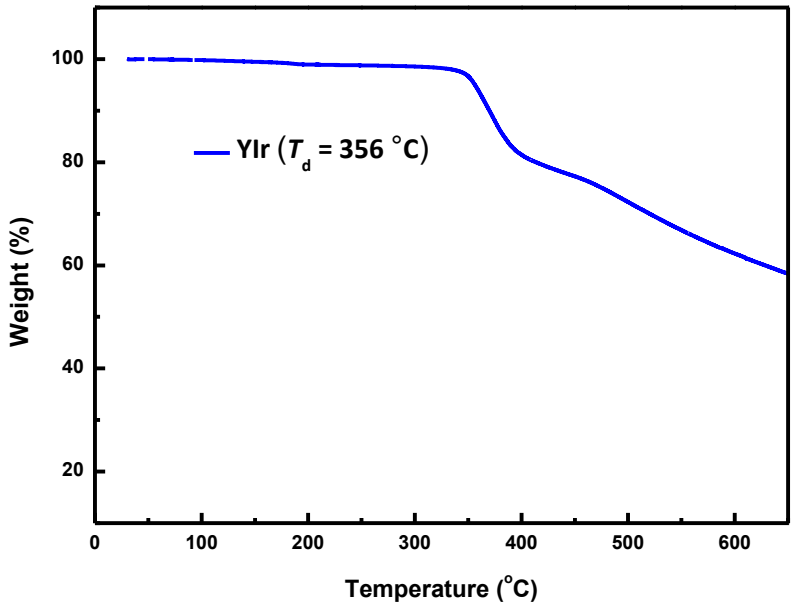

Figure 1. TGA data of **YIr** under N_2 atmosphere at a heating rate of 10 °C min^{-1}.

二、 Solution Photophysics

The UV-Vis and photo-induced luminescence (PL) spectra of complex **YIr** in MeCN solution at room temperature is shown in **Figure2**. The complex exhibits different excited states and has a high absorbance in the range of about 250–300 nm, which are ascribed to spin-allowed ligand-centered $\pi \rightarrow \pi^*$ transitions of both cyclometalated and ancillary ligands. The longer wavelength signals between 300 and 400 nm can be assigned to spin-allowed metal-to-ligand (MLCT) and ligand-to-ligand charge transfer (LLCT) excitations, whereas the weak intensity bands above 400 nm correspond to spin-forbidden MLCT, LLCT, and ligand-centered (LC) electronic transitions.[1,3] The detailed photophysical and characteristics of complex **YIr** is summarized in **Table 1**. The PL spectrum of complex **YIr** in aerated MeCN solution shows broad and featureless spectra at room temperature, indicating that the emission is related with MLCT rather than LC transitions.[4,5] The steep intensities of the spin-forbidden MLCT band arise from the strong spin-orbit coupling of the heavy iridium atom which in turn causes the mixing with higher lying MLCT transition states. The emission centered at 602 nm corresponds to the light emission in the yellow region. In addition, the shape and

position of the emission band is independent of the excitation wavelength. The phosphorescent nature of complex **YIr** is supported by lifetime of almost 1 μs (824 ns) in degassed MeCN (**Figure 3**).

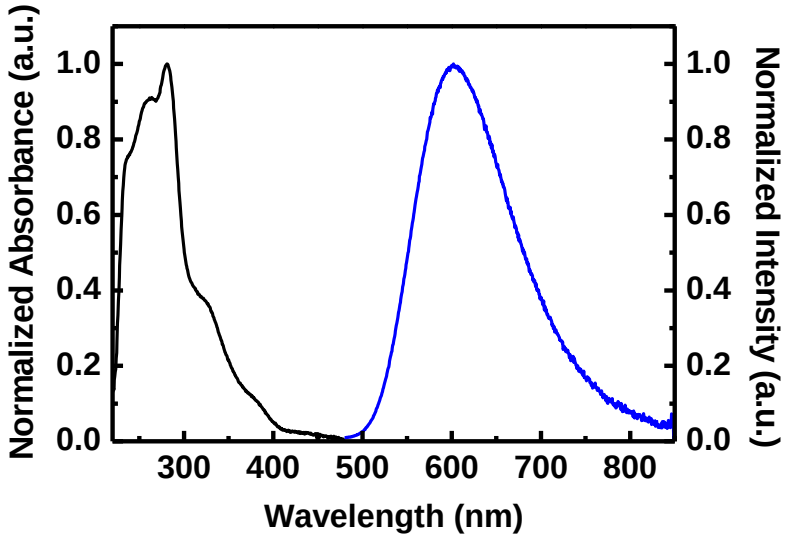

Figure 2. Absorption (black) and PL spectra (blue) of complex **YIr** in MeCN solution (1.0×10^{-5} M).

Table 1. Summary of selected physical properties of complex **YIr**.

Complex	Absorption [nm][a]	Emission [nm][a]	Φ_{PL} [%][b]	τ_{obs} [ns][c]	$E_{1/2}^{ox}$ [V][d]	Electrochemical [eV]			TD-DFT [eV]			Optical [eV][e]	T_d [°C][f]
						HOMO	LUMO[e]	*E*g	HOMO	LUMO	*E*g	*E*g	
YIr	264, 281	602	61	824	1.38	-5.70	-3.27	2.43	-6.00	-3.52	2.48	2.48	356

[a]Measured in 1×10^{-5} M MeCN at room temperature. [b]Solid-state absolute quantum yield was measured by employing an integrating sphere. [c]Lifetime measurement was carried out in degassed MeCN (1×10^{-5} M, λ_{ex} = 365 nm). [d]$TBAPF_6$ (0.1 M) was used as electrolyte in MeCN. Potential vs. ferrocene/ferrocenium redox couple. [e]Derived from the onset of emission wavelength. [f]Temperature at 5% weight loss to initial weight.

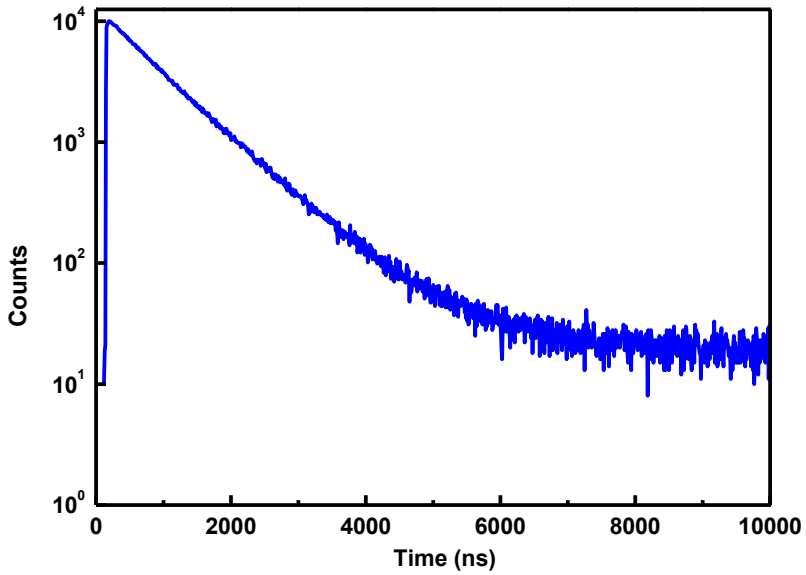

Figure 3. Phosphorescence decay of cationic iridium complex **YIr**.

三、 Electrochemical Properties and Theoretical Calculations

CV studies of complex **YIr** revealed redox waves, and the acquired electrochemical data are summarized in **Table 1**, with cyclic voltammogram depicted in **Figure 4**. The reversible oxidation potentials (highest occupied molecular orbital, HOMO) of complex **YIr** was measured in MeCN solvent, and the redox potential of ferrocene (Fc/Fc^+) was used as the standard. The lowest unoccupied molecular orbital (LUMO) level was derived from the onset of the emission band which suggest hole and electrons are transported during the operation of the LEC device. According to the onset of the oxidation potential, the HOMO level of **YIr** measured at -5.70 eV, with the credible LUMO level of -3.27 eV. The LUMO level was derived from the optical gap calculated from the corresponding HOMO level and the absorption onset value in solution PL spectrum. In addition, TD-DFT calculations were carry out to obtain further insight into the photophysical and electrochemical behaviors of the cationic complex. The geometry of the complex was optimized by using B3LYP functional. The iridium atom was treated by the LANL2DZ basis set while all the other atoms were

treated by 6-31G(d,p) basis set. The ground state geometry of complex **YIr** is shown in **Figure 5**a and the optimized geometry together with molecule surfaces of complex **YIr** in ground state is shown in **Figure 5**b. Based on the results of TD-DFT calculations, the HOMO is -6.00 (eV) which mostly located on the iridium center and the C^N ligand, and the LUMO is -3.52 (eV) which primarily distributed on the N^N ligand. In comparing the energy levels and energy gaps from the TD-DFT calculations, CV measurements and emission spectrum, the similar values can be observed (cf. **Table 1**).

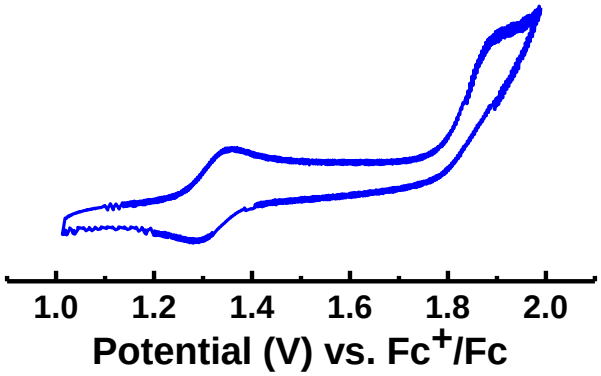

Figure 4. Cyclic voltammogram of complex **YIr** in MeCN solution. Potential was recorded versus Fc^+/Fc.

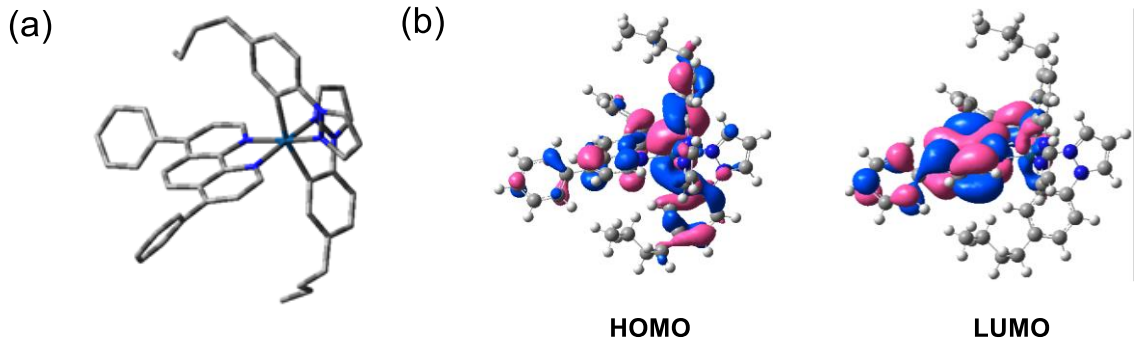

Figure 5. a) Ground state geometries of complex **YIr** obtain at B3LYP/6-31G(d,p)/LANL2DZ level of theory. Hydrogen atoms are omitted for clarity. b) Electron density distribution pattern of the frontier molecular orbitals for complex **YIr**.

伍、 討論

To test the EL properties of complex **YIr**, the guest-only LEC (80 wt.% complex **YIr** and 20 wt.% [$BMIM^+(PF_6)^-$]) was fabricated and the EL characteristics are summarized in **Table 2**. The EL spectrum of the guest-only LEC is shown in **Figure 6**. The orange EL emission peak of complex **YIr** locates at 605 nm, which is similar to the PL emission of complex **YIr** in MeCN solution (**Figure 2**). Time-dependent voltage, brightness and EQE of the guest-only LEC under constant driving currents are shown in **Figure 7**a, **7**b and **7**c, respectively. The required voltage to drive the LEC at a constant current is initially high due to the high carrier injection barrier from the electrode into the undoped emissive layer. When the electrochemically doped layers are gradually formed, the carrier injection barrier lowers and the required voltage to maintain the same current reduces significantly. In the steady state, the device voltage approaches constant at *ca.* 2.4 V. Device brightness increases with time due to the improved balance in electron and hole currents. After reaching the maximal brightness, gradually reduced brightness is attributed to exciton quenching in the proximity of expanding p- and n-type doped layers[58,59] and/or emissive material degradation.[60] The EQE of the LEC follows similar temporal evolution trend as brightness since it is driven under a constant current. The peak EQE of the guest-only LEC is up to 13.6%. High device efficiency of the guest-only LEC partially results from high PLQY of its emissive layer (*ca.* 61%). Bulky phenyl groups on the phenanthroline ligand of complex **YIr** reduce intermolecular interactions between complexes[61] and highly retained PLQY in thin film can be obtained. To examine carrier balance of the guest-only LEC, the optical simulation tool (Setfos, FLUXiM)[62] was employed to fit the simulated spectrum with the measured EL spectrum by adjusting the emission zone position in optical simulation. The emission zone position can thus be estimated when the spectrum generated by optical simulation matches well with the measured EL spectrum.[30,34,35,40,45,63,64] With the emission zone position in an LEC, the percentages of optical modes can be calculated, including the light outcoupling efficiency. In optical simulation, the emissive-layer

thickness of the gust-only LEC was 145 nm and the emission zone profile was assumed to be Gaussian with a full width half maximum (FWHM) of 20 nm. The fitted simulated and measured EL spectra of the guest-only LEC are shown in **Figure 8**a. The related emission zone position (100 nm from cathode) in the emissive layer of the guest-only LEC is illustrated in **Figure 7**a. The emission zone position in the guest-only LEC is closer to the anode and the carrier balance may not be perfect in spite of its high device efficiency. To quantize carrier balance, the device EQE can be determined by the factors shown in the following equation.

$$\eta_{EQE} = \eta_{out} \times \gamma \times \eta_{S,T} \times \eta_{QY}$$

In this equation, η_{EQE} is the measured EQE of LEC, η_{out} is the light outcoupling efficiency, γ is the factor of carrier balance, $\eta_{S,T}$ is the emissive exciton generation efficiency and η_{QY} is the PLQY of the emissive layer of LEC. For phosphorescent materials, the emissive exciton generation efficiency $\eta_{S,T}$ can be considered as unity since all electron-hole pairs can generate emissive triplet excitons. The light outcoupling efficiency η_{out} can be calculated by optical simulation. With measured device EQE and PLQY of the emissive layer, the factor of carrier balance γ can be estimated. These factors for the guest-only LEC are listed in **Table 3**. The relatively lower γ value of *ca.* 81% confirms imperfect carrier balance of the guest-only LEC. The emission zone position closer to the anode implies better electron transport than hole transport in the guest-only emissive layer (**Figure 7**a). High electron mobility reported for the phenanthroline derivative (bathophenanthroline), which is the ligand of complex **YIr**, supports this point.[65] As such, further optimization is required to obtain better device efficiency.

Table 2. Summary of the device EL characteristics of the host-guest LECs under constant currents.

Complex **YIr** [wt.%][a)]	Current [μA][b)]	EL_{max} [nm][c)]	CIE [x, y][d)]	B_{max} [cd m^{-2}][e)]	$\eta_{ext,max}$ [%][f)]	$\eta_{c,max}$ [cd A^{-1}][g)]	$\eta_{P,max}$ [lm W^{-1}][h)]
10[i)]	0.1	568	(0.47, 0.52)	4.2	13.3	41.7	38.6

20[i)]	0.1	575	(0.49, 0.50)	4.8	16.9	48.3	57.1
40[i)]	0.5	587	(0.53, 0.47)	19.9	15.9	39.7	49.4
60[i)]	0.5	594	(0.54, 0.46)	18.2	15.3	36.4	47.4
80[i)]	1	605	(0.56, 0.44)	27.3	13.6	27.3	36.1
20[j)]	0.1	566 to 599[k)]	(0.45, 0.53) to (0.56, 0.43)[k)]	4.3	11.9	42.9	47.9
20[j,l)]	0.1	565	(0.47, 0.52)	7.0	23.7	69.9	81.2

[a)]Components of the emissive layer: complex **BG** (80-x wt.%), complex **YIr** (x wt.%) and $BMIM^+PF_6^-$ (20 wt.%). [b)]The device current to reach the maximal device efficiency. [c)]EL peak wavelength. [d)]Commission Internationale de l'Eclairage (CIE) 1931 coordinates. [e)]Maximal brightness. [f)]Maximal external quantum efficiency. [g)]Maximal current efficiency. [h)]Maximal power efficiency. [i)]Thickness of the emissive layer is *ca.* 145 nm. [j)]Thickness of the emissive layer is *ca.* 490 nm. [k)]EL spectrum changes with time. [l)]With a diffusive layer between ITO and glass substrate.

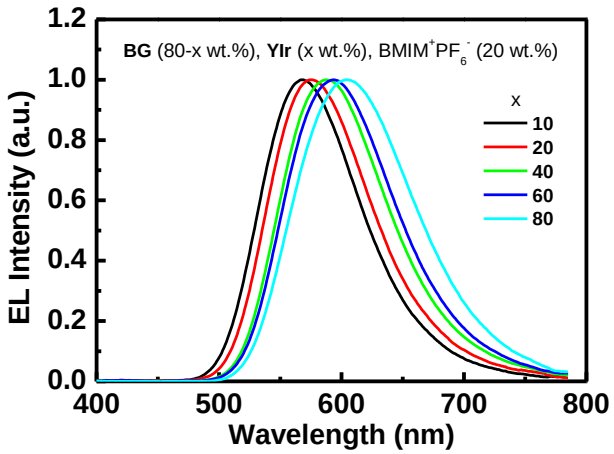

Figure 6. EL spectra of the host-guest LECs (145 nm) based on complex **BG** doped with complex **YIr**.

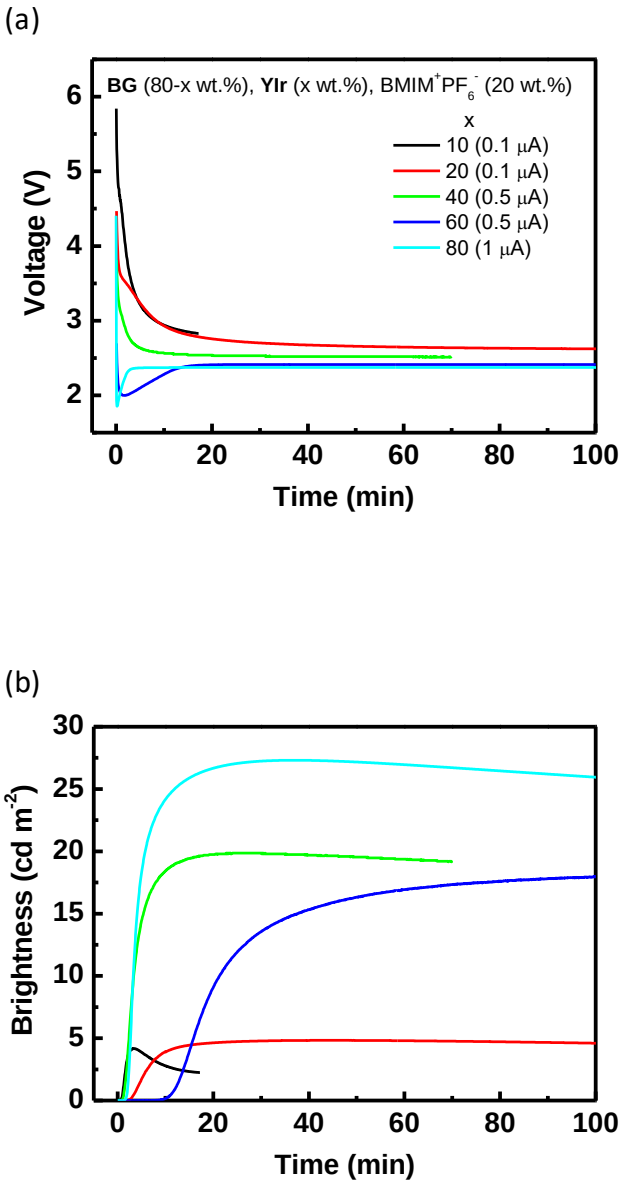

Figure 7. Time-dependent a) voltage, b) brightness and c) EQE of the host-guest LECs (145 nm) based on complex **BG** doped with complex **YIr** under constant currents.

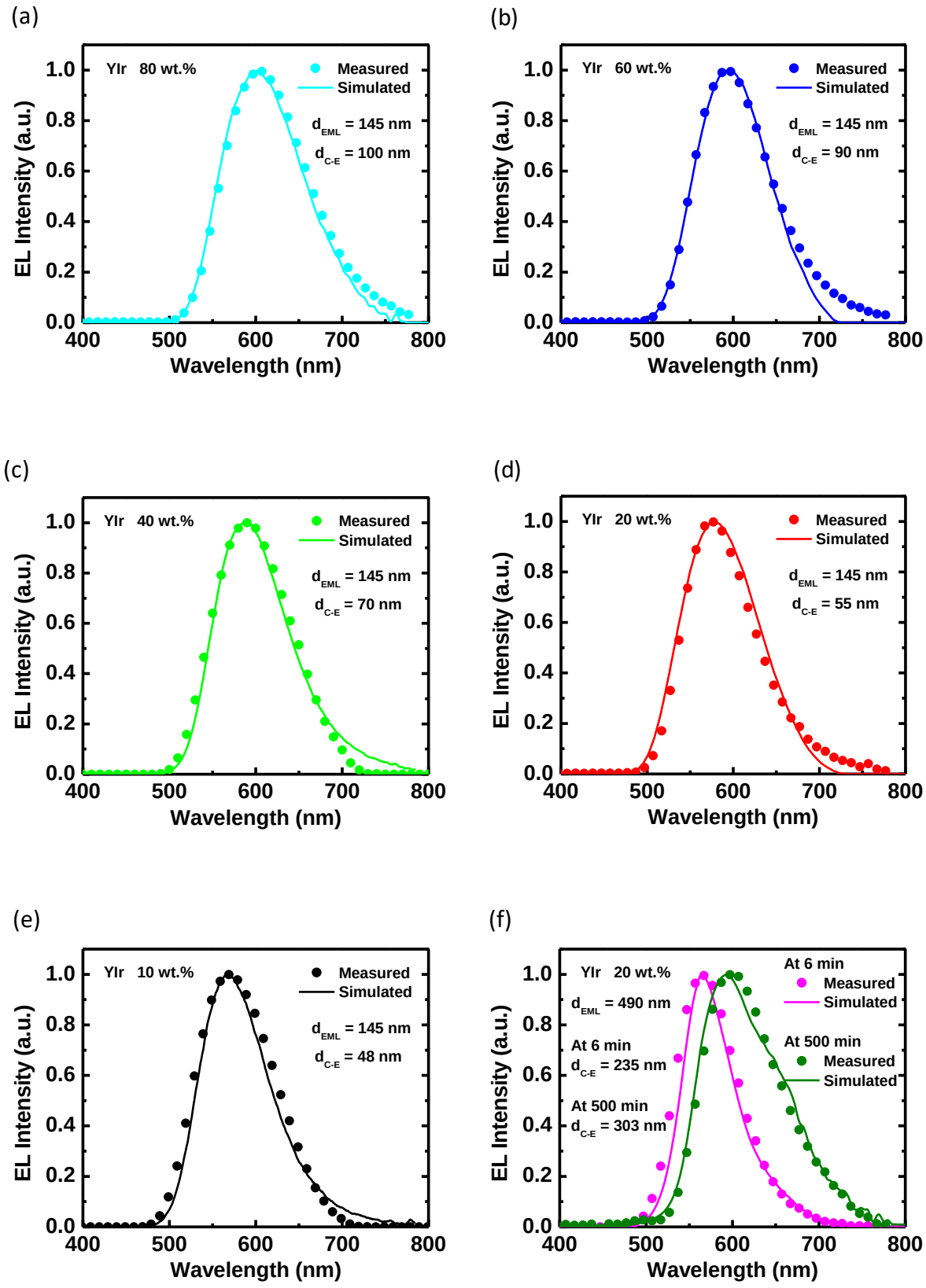

Figure 8. Simulated (line) and measured (solid symbol) EL spectra of the host-guest LECs based on complex **BG** doped with complex **YIr** at a) 80, b) 60, c) 40, d) 20, e) 10 and f) 20 wt.%. The emissive–layer thickness is 145 nm for a)–e) and 490 nm for f). The estimated emission zone position from

cathode (d_{C-E}) is labeled on each subfigure.

To reduce self-quenching effect of guest molecules and to further improve carrier balance, the host complex **BG** was incorporated in the guest-only LEC and the EL characteristics of the host-guest LECs with various concentrations of the guest complex **YIr** are summarized in **Table 2**. The emissive-layer thickness (d_{EML}) of the host-guest LEC is the same as that of the guest-only LEC (145 nm). The EL spectra of the host-guest LECs are shown in **Figure 6**. The EL emission peak is blue-shifted since incorporation of the host complex reduces intermolecular interactions between guest complex molecules. Under constant-current driving, the host-guest LECs show similar temporal evolution in voltage, brightness and EQE to the guest-only LEC (**Figure 7**a–c). However, the stabilized voltage slightly increases as the weight percentage of the higher-gap host complex increases (**Figure 7**a). In addition, the peak EQE of the host-guest LECs increases as the concentration of guest complex decreases (80 to 20 wt.%, **Table 2**). The maximal EQE up to 16.9% can be obtained when 20 wt.% guest complex is employed. Further decreasing the concentration of guest complex (10 wt.%) results in a lower EQE. The emission zones of the host-guest LECs were estimated by fitting the measured EL spectra with the spectra generated by optical simulation. The fitted EL spectra along with the estimated emission zone positions from cathode (d_{C-E}) for the host-guest LECs doped with guest complex **YIr** at 60, 40, 20 and 10 wt.% are shown in **Figure 8**b, **8**c, **8**d and **8**e, respectively. As shown in **Figure 9**a, the emission zone position moves towards the anode when the concentration of guest complex increases. It is related to the energy-level alignments of the host and guest complexes. The host-guest energy offset is higher in the HOMO levels than in the LUMO levels (**Figure 10**). Therefore, a higher concentration of the guest complex results in more significant hole trapping than electron trapping, rendering an emission zone moving towards the anode. Similar shift of emission zone has been observed in the red LECs employing the host complex **BG** doped with a red-emitting complex.[19] To examine carrier balance of the host-guest LECs doped with various concentrations of guest complex, the factors of carrier balance for the host-guest LECs were calculated and the related

factors are listed in **Table 3**. The factor of carrier balance γ increases as the emission zone moves towards the center of the emissive layer. The best factor of carrier balance (*ca.* 92%) corresponds to the host-guest LEC doped with 20 wt.% guest complex **YIr**, which also shows the highest EQE (16.9%). Compared with the guest-only LEC, *ca.* 24% enhancement in EQE can be achieved in the optimized host-guest LEC. In addition to improved carrier balance, enhanced PLQY (from *ca.* 61 to 73%, **Table 3**) of the dispersed guest molecules in the host-guest emissive layer also contributes to the increased EQE. It is noted that the emission zone position of the host-guest LEC (20 wt.% guest complex **YIr**) showing the best carrier balance is not perfectly located at the center of the emissive layer, but is slightly closer to the cathode (d_{C-E}/d_{EML} = 38%, **Figure 9**a). It may be attributed to asymmetric p- and n-type doped layers[64,66] and the emission zone is slightly off-centered when the carrier balance is optimized.

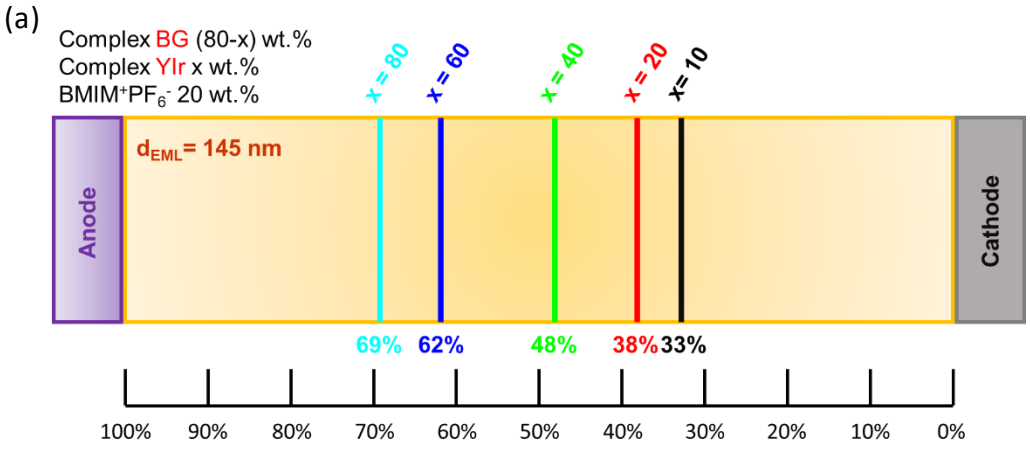

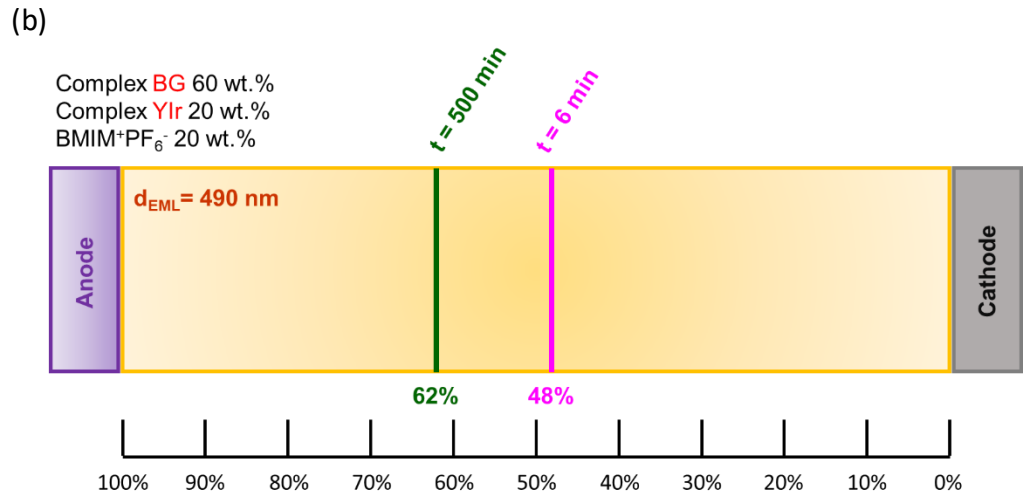

Figure 9. Schematic diagrams of the relative emission zone position in the emissive layer for a) the host-guest LECs (145 nm) based on complex **BG** doped with complex **YIr** at 10, 20, 40, 60 and 80 wt.% and b) the host-guest LECs (490 nm) based on complex **BG** doped with complex **YIr** at 20 wt.% after operation of 6 and 500 min.

Table 3. Summary of the factors associated with the carrier balance of host-guest LECs under constant currents.

Complex **YIr** [wt.%][a)]	Current [μA][b)]	η_{EQE} [%][c)]	η_{out} [%][d)]	γ [%][e)]	$\eta_{S,T}$ [%][f)]	η_{QY} [%][g)]	d_{C-E}/d_{EML} [%][h)]
10[i)]	0.1	13.3	21.9	80.4	100	75.5	33
20[i)]	0.1	16.9	25.0	92.2	100	73.3	38
40[i)]	0.5	15.9	28.7	84.6	100	65.5	48
60[i)]	0.5	15.3	31.9	83.1	100	57.7	62
80[i)]	1	13.6	27.8	80.7	100	60.6	69
20[j)]	0.1	11.9	22.4	72.5	100	73.3	48 to 62[k)]
20[i,l)]	0.1	23.7	44.6	72.5	100	73.3	48 to 62[k)]

[a)]Components of the emissive layer: complex **BG** (80-x wt.%), complex **YIr** (x wt.%) and $BMIM^+PF_6^-$ (20 wt.%). [b)]The device current to reach the maximal device efficiency. [c)]External quantum efficiency. [d)]Light outcoupling efficiency.

[e)]Factor of carrier balance. [f)]Emissive exciton generation efficiency. [g)]Photoluminescence quantum yield. [h)]d_{C-E}: emission zone position from cathode. d_{EML}: thickness of emissive layer. [i)]Thickness of the emissive layer is *ca.* 145 nm. [j)]Thickness of the emissive layer is *ca.* 490 nm. [k)]Emission zone moves with time. [l)] With a diffusive layer between ITO and glass substrate.

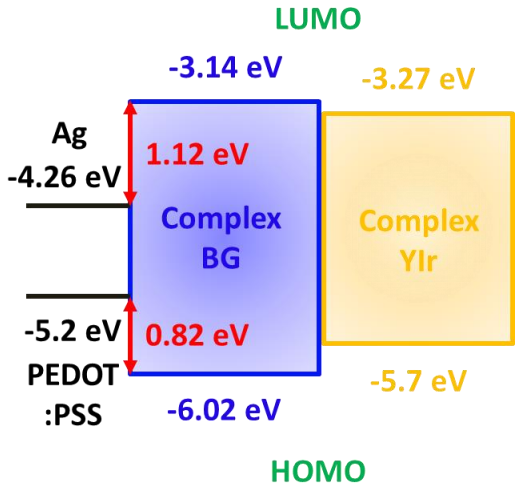

Figure 10. HOMO and LUMO energy levels of complex **BG** and complex **YIr**. The work functions of PEDOT:PSS and Ag are shown to facilitate evaluation of initial hole and electron injection barriers, respectively.

After optimizing carrier balance of the host-guest LEC, the device efficiency can be further improved by recycling the trapped light in the layered structure. Glass substrates with embedded diffusive layers containing scattering TiO_2 (NPs)[20] were employed to perform light extraction from LEC devices. The average roughness (R_a) value of the sputtered ITO layer on the diffusive layer is *ca.* 30 nm.[20] Large leakage currents were measured in thin LECs (145 nm) fabricated on the substrate containing a diffusive layer and the reproducibility of the EL characteristics is poor. Furthermore, the optical mode distribution in a thin LEC (145 nm) is not beneficial for light extraction with a diffusive layer. Based on the optical simulation performed by Setfos, the contribution of the optical mode versus emission zone position (from cathode) in the host-guest LECs (145 nm) based on complex **BG** doped with complex **YIr** at 20 wt.% is shown in **Figure 11**. With the emission zone position estimated

from **Figure 8**d (d_{C-E} = 55 nm), more than half of the total EL is coupled into surface plasmon mode. Short distance between the emission zone and cathode facilitates such coupling. The percentage of the EL in substrate mode, which can be scattered for light extraction, is lower than 20% such that the light outcoupling enhancement is limited. To improve device reproducibility and to increase light outcoupling, thick LECs (490 nm) were employed in the study of light extraction. The EL properties of the thick host-guest LECs (490 nm) based on complex **BG** doped with complex **YIr** at 20 wt.% are summarized in **Table 2**. In contrast to stable EL spectra of the thin LECs (145 nm) (**Figure 8**a–e), the EL spectrum of the thick LECs (490 nm) changes with time (**Figure 8**f). Initially, the EL peak is at 566 nm and it gradually moves to 598 when the EL spectrum is stabilized. It is attributed to altered microcavity effect induced by moving emission zone in an LEC under operation.[30,34,40,45,63,64] By fitting the spectra generated by optical simulation with the measured EL spectra, moving emission zone from d_{C-E} = 235 (6 min) to 303 nm (500 min) can be estimated (**Figure 8**f). In optical simulation of the thick LEC (490 nm), the emission zone profile was assumed to be Gaussian with a FWHM of 40 nm. The relative emission zone positions at 6 and 500 min in the emissive layer of the host-guest LECs (490 nm) based on complex **BG** doped with complex **YIr** at 20 wt.% are depicted in **Figure 9**b. The emission zone is initially at the center of the emissive layer and subsequently it moves towards the anode with time. Such trend of temporal evolution of emission zone can be explained by the energy level alignments shown in **Figure 10**. The hole injection barrier (0.82 eV) is much lower than the electron injection barrier (1.12 eV). The required amount of accumulated ions near the anode to achieve ohmic contact for hole is smaller than that required to achieve ohmic contact for electron at the cathode. Therefore, a longer time is required for electron injection efficiency to reach the maximal steady state under formation of the electrochemically doped layers, rendering an emission zone moving towards the anode. The peak EQE (11.9%) takes place shortly after the constant current is applied (*ca.* 6 min). The factor of carrier balance of the thick host-guest LEC (490 nm) is calculated to be *ca.* 73%, which is lower than that (*ca.* 92%) of the thin host-guest LEC (145 nm) with the same concentration of complex **YIr** (20 wt.%) (**Table 3**). In spite of the centered emission zone,

deteriorated carrier balance implies more significant asymmetric p- and n-type doped layers in the thick LEC. The contribution of the optical mode versus emission zone position (from cathode) in the host-guest LECs (490 nm) based on complex **BG** doped with complex **YIr** at 20 wt.% is shown in **Figure 12**. With the emission zone position at 6 min (d_{C-E} = 235 nm, **Figure 8**f) for the peak EQE, the percentage of surface plasmon mode is significantly reduced to <10% in the thick LEC (490 nm) due to increased distance between emission zone and electrode. Furthermore, the percentage of substrate mode increases substantially to *ca.* 60%. Large proportion of EL in substrate mode is beneficial for light extraction. Therefore, the EQE and power efficiency of the thick LEC (490 nm) integrated with the embedded diffusive layer reach 23.7% and 81.2 lm W^{-1}, respectively. Based on the measured device EQE, PLQY of the emissive layer and estimated factor of carrier balance mentioned above, the light outcoupling efficiency (η_{out}) of the thick LEC (490 nm) is calculated to be enhanced to *ca.* 45% by utilizing the embedded diffusive layer (**Table 3**). The diffusive layer almost doubles the light outcoupling efficiency of the thick LEC. Similar enhancement ratios in light outcoupling efficiency were reported in blue and white LECs based on the same embedded diffusive layers.[20] Compared with the guest-only LEC, 1.74X enhancement in device efficiency is achieved. These results confirm that both optimizations of carrier balance and light extraction are effective in realizing highly efficient LECs. In addition to enhanced device efficiency, stable EL spectrum can be measured in the LEC employing the substrate with an embedded diffusive layer (**Figure 13**). The diffusive layer destroys the resonant optical feedback from glass/air interface such that the influence of microcavity effect on the output EL spectrum when the emission zone in an LEC is moving can eliminated. As such, the EL spectrum is stabilized and turns into the intrinsic emission spectrum of the emissive layer

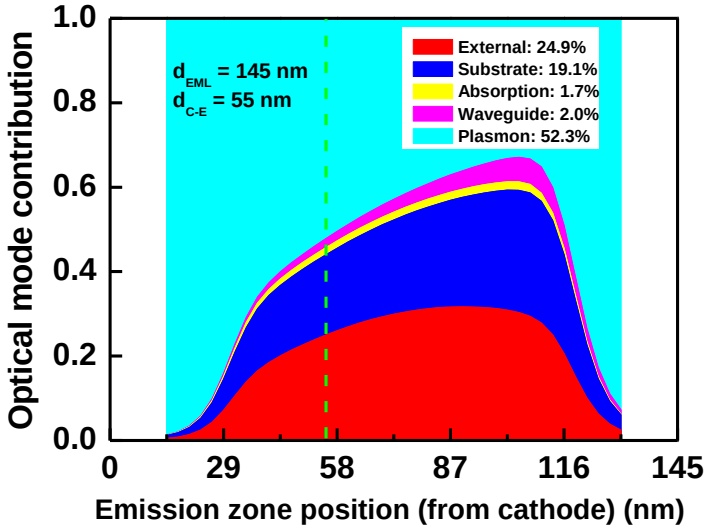

Figure 11. Simulated contribution of each optical mode versus emission zone position in the host-guest LECs (145 nm) based on complex **BG** doped with complex **YIr** at 20 wt.%. The emission zone position from cathode (d_{C-E}) is labeled to facilitate evaluating the optical mode contribution shown in the inset.

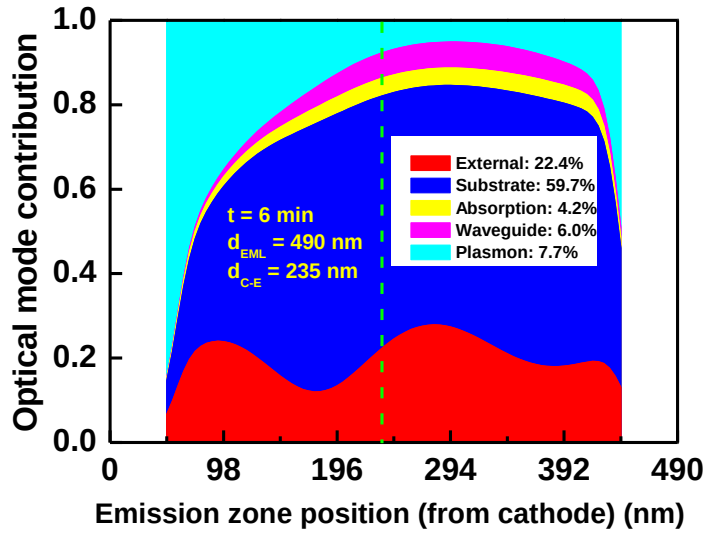

Figure 12. Simulated contribution of each optical mode versus emission zone position in the host-guest LECs (490 nm) based on complex **BG** doped with complex **YIr** at 20 wt.%. The emission zone position from cathode (d_{C-E}) at 6 min is labeled to facilitate evaluating the optical mode contribution shown in the inset.

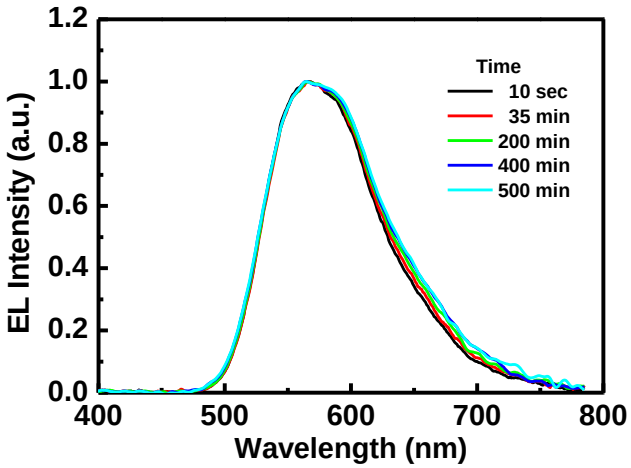

Figure 13. EL spectra of the host-guest LECs (490 nm) based on complex **BG** doped with complex **YIr** at 20 wt.% on the substrate embedded with a diffusive layer.

陸、 結論

我們利用了 **YIr** 的剛性、載流子平衡優化和光提取等技術，實現超高效率 LECs 元件。本研究使用正丁基搭配苯基吡唑作為供電子基團的 C^N 配體，將具有較長共軛體系的 4,7-二苯基-1,10-菲咯啉作為接受電子基團的 N^N 配體，合成為橘黃光銥金屬錯合物 **YIr**。此外，錯合物 **YIr** 具有苯基及長碳鏈而有著高度的立體障礙，因此在薄膜狀態下保留高達 61% 的 PLQY。錯合物 **YIr** 於無摻雜 LECs 元件表現出良好的載流子平衡（γ = 81%），EQE 達到 13.6 %。為了更進一步提高載流子平衡並降低分子間自我猝滅效應，我們將錯合物 **YIr** 分散在藍綠光之主體錯合物 **BG** 中，形成一個主-客體系統的 LECs 放光層，比對了不同比例的摻雜結果，可看出當比例為 20 wt%時具有最高的元件效率表現，包含載流子平衡（γ = 92%）、73% 的 PLQY 及 16.9%的 EQE。此外，本研究通過添加擴散層來實現光提取的增強，發現於厚元件中的主-客體 LECs 的 EQE 高達 23.7%，這是非常優異的元件表現，與目前的 LECs 相比，達到 174%的元件效率提升，甚至可媲美 OLEDs，如此高的 EQE 證明了我們所提出的組合方法（包括採用有效的發光材料、優化載流子平衡以及增加光提取量）是非常具潛力實現超高效率 LECs。

柒、 參考資料及其他

[1] Tang, C. W.; VanSlyke, S. A. Organic Electroluminescent Diodes. *Appl. Phys. Lett*. **1987**, *51*, 913-915.

[2] Pei, Q.; Yu, G.; Zhang, C.; Yang, Y.; Heeger, A. J. Polymer Light-Emitting Electrochemical Cells. *Science.* **1995**, *269*, 1086-1088.

[3] Tang, S.; Edman, L. Light-Emitting Electrochemical Cells: A Review on Recent Progress. *Top. Curr. Chem*. **2016**, *374*, 40.

[4] Lee, J. K.; Yoo, D. S.; Handy, E. S.; Rubner, M. F. Thin Film Light Emitting Devices from an Electroluminescent Ruthenium Complex. *Appl. Phys. Lett*. **1996**, *69*, 1686-1688.

[5] Slinker, J. D.; Gorodetsky, A. A.; Lowry, M. S.; Wang, J. J.; Parker, S.; Rohl, R.; Bernhard, S.; Malliaras, G. G. Efficient Yellow Electroluminescence from a Single Layer of a Cyclometalated Iridium Complex. *J. Am. Chem*. **2004**, *126*, 2763-2767.

[6] Costa, R. D.; Orti, E.; Bolink, H. J.; Monti, F.; Accorsi, G.; Armaroli, N. Luminescent Ionic Transition-Metal Complexes for Light-Emitting Electrochemical Cells. *Angew. Chem. Int. Ed.* **2012**, *51*, 8178-8211.

[7] Fresta, E.; Costa, R. D. Beyond Traditional Light-Emitting Electrochemical Cells – A Review of New Device Designs and Emitters. *J. Mater. Chem. C*. **2017**, *5*, 5643-5675.

[8] Hill, Z. B.; Rodovsky, D. B.; Leger, J. M.; Bartholomew, G. P. Synthesis and Utilization of Perylene-Based N-Type Small Molecules in Light-Emitting Electrochemical Cells. *Chem. Commun.* **2008**, 6594-6596.

[9] Bader, A. J. N.; Ilkevich, A. A.; Kosilkin, I. V.; Leger, J. M. Precise Color Tuning via Hybrid Light-Emitting Electrochemical Cells. *Nano Lett*. **2011**, *11*, 461-465.

[10] Aygüler, M. F.; Puscher, B. M. D.; Tong, Y.; Bein, T.; Urban, A.; Costa, R. D.; Docampo, P. Light-Emitting Electrochemical Cells Based on Inorganic Metal Halide Perovskite Nanocrystals. *J. Phys. D-Appl. Phys.* **2018**, *51*, 334001.

[11] Zhang, Q.; Zhou, Q.; Cheng, Y.; Wang, L.; Ma, D.; Jing, X.; Wang, F. Highly Efficient Electroluminescence from Green-Light-Emitting Electrochemical Cells Based on CuI Complexes. *Adv. Funct. Mater.* **2006**, *16*, 1203-1208.

[12] Su, H.-C.; Wu, C.-C.; Fang, F.-C.; Wong, K.-T. Efficient Solid-State Host-Guest Light-Emitting Electrochemical Cells Based on Cationic Transition Metal Complexes. *Appl. Phys. Lett.* **2006**, *89*, 261118.

[13] Bolink, H. J.; Coronado, E.; Costa, R. D.; Lardies, N.; Ortí, E. Near-Quantitative Internal Quantum Efficiency in a Light-Emitting Electrochemical Cell. *Inorg. Chem.* **2008**, *47*, 9149-9151.

[14] Wu, H.-B.; Chen, H.-F.; Liao, C.-T.; Su, H.-C.; Wong, K.-T. Efficient and Color-Stable Solid-State White Light-Emitting Electrochemical Cells Employing Red Color Conversion Layers. *Org. Electron.* **2012**, *13*, 483-490.

[15] Zhang, J.; Zhou, L.; Al-Attar, H. A.; Shao, K.; Wang, L.; Zhu, D.; Su, Z.; Bryce, M. R.; Monkman, A. P. Efficient Light-Emitting Electrochemical Cells (LECs) Based on Ionic Iridium(III) Complexes with 1,3,4-Oxadiazole Ligands. *Adv. Funct. Mater.* **2013**, *23*, 4667-4677.

[16] Zanoni, K. P. S.; Sanematsu, M. S.; Iha, N. Y. M. Photophysical Characterization of $[Ir(ppy)_2(dmb)][PF_6]$ Towards Application in Light-Emitting Electrochemical Cells (LECs). *Inorg. Chem. Commun.* **2014**, *43*, 162-164.

[17] Lin, G.-R.; Cheng, J.-R.; Wang, C.-W.; Sarma, M.; Chen, H.-F.; Su, H.-C.; Chang, C.-H.; Wong, K.-T. Solid-State White Light-Emitting Electrochemical Cells Based on Scattering Red Color Conversion Layers. *J. Mater. Chem. C.* **2015**, *3*, 12492-12498.

[18] Cheng, C.-Y.; Wang, C.-W.; Cheng, J.-R.; Chen, H.-F.; Yeh, Y.-S.; Su, H.-C.; Chang, C.-H.; Wong, K.-T. Enhancing Device Efficiencies of Solid-State White Light-Emitting Electrochemical Cells by Employing Waveguide Coupling. *J. Mater. Chem. C.* **2015**, *3*, 5665-5673.

[19] Yu, G.-X.; Lin, C.-H.; Liu, Y.-X.; Yi, R.-H.; Chen, G.-Y.; Lu, C.-W.; Su, H.-C. Efficient and Saturated Red Light-Emitting Electrochemical Cells Based on Cationic Iridium(III) Complexes with EQE up to 9.4%. *Chem. Eur. J.* **2019**, *25*, 13748-13758.

[20] Chen, Y.-Z.; Luo, D.; Hsiang, C.-H.; Yi, R.-H.; Lin, C.-H.; Lu, C.-W.; Liu, S.-W.; Chang, C.-H.; Su, H.-C. Highly Efficient Blue and White Light-Emitting Electrochemical Cells Employing Substrates Containing Embedded Diffusive Layers. *Org. Electron. DOI: 10.1016/j.orgel.***2019**.105515.

[21] Liao, C.-T.; Chen, H.-F.; Su, H.-C.; Wong, K.-T. Tailoring Balance of Carrier Mobilities in Solid-State Light-Emitting Electrochemical Cells by Doping a Carrier Trapper to Enhance Device Efficiencies. *J. Mater. Chem*. **2011**, *21*, 17855-17862.

[22] Su, H.-C.; Chen, H.-F.; Shen, Y.-C.; Liao, C.-T.; Wong, K.-T. Highly Efficient Double-Doped Solid-State White Light-Emitting Electrochemical Cells. *J. Mater. Chem*. **2011**, *21*, 9653-9660.

[23] Marcantonio, M. D.; Vollkommer, F.; Bacherc, G.; Nannen, E. A Light-Emitting Electrochemical Cell (LEC) Containing a Hole-Blocking Layer of TmPyPB. *J. Mater. Chem. C*. **2018**, *6*, 9742-9748.

[24] Liao, C.-T.; Chen, H.-F.; Su, H.-C.; Wong, K.-T. Tailoring Carrier Injection Efficiency to Improve the Carrier Balance of Solid-State Light-Emitting Electrochemical Cells. *Phys. Chem. Chem. Phys.* **2012**, *14*, 9774-9784.

[25] Roldán-Carmona, C.; Akatsuka, T.; Sessolo, M.; Watkins, S. E.; Bolink, H. J. Engineering Charge Injection Interfaces in Hybrid Light-Emitting Electrochemical Cells. *ACS Appl. Mater. Interfaces* **2014**, *6*, 19520-19524.

[26] Xu, J.; Sandström, A.; Lindh, E. M.; Yang, W.; Tang, S.; Edman, L. Challenging Conventional Wisdom: Finding High-Performance Electrodes for Light-Emitting Electrochemical Cells. *ACS Appl. Mater. Interfaces*. **2018**, *10*, 33380-33389.

[27] He, L.; Wang, X.; Duan, L. Enhancing the Overall Performances of Blue Light-Emitting Electrochemical Cells by Using an Electron-Injecting/Transporting Ionic Additive. *ACS Appl. Mater. Interfaces.* **2018**, *10*, 11801-11809.

[28] Hu, Y.; Gao, J. Cationic Effects in Polymer Light-Emitting Electrochemical Cells. *Appl. Phys. Lett*. **2006**, *89*, 253514.

[29] Shen, Y.; Kuddes, D. D.; Naquin, C. A.; Hesterberg, T. W.; Kusmierz, C.; Holliday, B. J.; Slinker,

J. D. Improving Light-emitting Electrochemical Cells with Ionic Additives. *Appl. Phys. Lett*. **2013**, *102*, 203305.

[30] Sun, R.; Liao, C.-T.; Su, H.-C. Effects of Incorporating Salts with Various Alkyl Chain Lengths on Carrier Balance of Light-Emitting Electrochemical Cells. *Org. Electron.* **2014**, *15*, 2885-2892.

[31] Bandiello, E.; Sessolo, M.; Bolink, H. J. Lithium Salt Additives and the Influence of Their counterion on the Performances of Light-Emitting Electrochemical Cells. *J. Mater. Chem. C.* **2016**, *4*, 10781-10785.

[32] Chen, H.-F.; Liao, C.-T.; Su, H.-C.; Yeh, Y.-S.; Wong, K.-T. Highly Efficient Exciplex Emission in Solid-State Light-Emitting Electrochemical Cells Based on Mixed Ionic Hole-Transport Triarylamine and Ionicelectron-Transport 1,3,5-Triazine Derivatives. *J. Mater. Chem. C.* **2013**, *1*, 4647-4654.

[33] Pertegás, A.; Shavaleev, N. M.; Tordera, D.; Ortí, E.; Nazeeruddin, M. K.; Bolink, H. J. Host-Guest Blue Light-Emitting Electrochemical Cells. *J. Mater. Chem. C.* **2014**, *2*, 1605-1611.

[34] Huang, P.-C.; Krucaite, G.; Su, H.-C.; Grigalevicius, S. Incorporating a Hole-Transport Material into The Emissive Layer of Solid-State Light-Emitting Electrochemical Cells to Improve Device Performance. *Phys. Chem. Chem. Phys.* **2015**, *17*, 17253-17259.

[35] Jhang, Y.-P.; Chen, H.-F.; Wu, H.-B.; Yeh, Y.-S.; Su, H.-C.; Wong, K.-T. Improving Device Efficiencies of Solid-State White Light-Emitting Electrochemical Cells by Adjusting the Emissive-Layer Thickness. *Org. Electron.* **2013**, *14*, 2424-2430.

[36] Li, X.; Gao, J.; Liu, G. Thickness Dependent Device Characteristics of Sandwich Polymer Light-Emitting Electrochemical Cell. *Org. Electron.* **2013**, *14*, 1441-1446.

[37] Lindh, E. M.; Lundberg, P.; Lanz, T.; Mindemark, J.; Edman, L. The Weak Micro Cavity as an Enabler for Bright and Fault-Tolerant Light-Emitting Electrochemical Cells. *Sci. Rep.* **2018**, *8*, 6970.

[38] Liu, C.-Y.; Bard, A. J. Highly Efficient and Bright Electroluminescent $Ru(bpy)_3(ClO_4)_2$/Alq_3 device. *Appl. Phys. Lett*. **2005**, *87*, 061110.

[39] Tang, S.; Sandström, A.; Fang, J.; Edman, L. A Solution-Processed Trilayer Electrochemical

Device: Localizing the Light Emission for Optimized Performance. *J. Am. Chem. Soc.* **2012**, *134*, 14050-14055.

[40] Lee, C.-L.; Cheng, C.-Y.; Su, H.-C. Enhancing Device Efficiencies of Solid-State Near-Infrared Light-Emitting Electrochemical Cells by Employing a Tandem Device Structure. *Org. Electron.* **2014**, *15*, 711-720.

[41] Su, H.-C.; Hsu, J.-H. Improving the Carrier Balance of Light-Emitting Electrochemical Cells Based on Ionic Transition Metal complexes. *Dalton Trans.* **2015**, *44*, 8330-8345.

[42] Kaihovirta, N.; Larsen, C.; Edman, L. Improving the Performance of Light-Emitting Electrochemical Cells by Optical Design. *ACS Appl. Mater. Interfaces.* **2014**, *6*, 2940-2947.

[43] Jang, Y.-F.; Lin, T.-C.; Guo, J.-Y.; Fan Chiang, C.-M.; Wu, M.-L.; Shen, H.-Y.; Chen, T.-C.; Yang, Z.-P.; Lee, Y.-J.; Su, H.-C.; Chang, C.-H.; Liu, S.-W. Enhancing Extracted Electroluminescence from Light-Emitting Electrochemical Cells by Employing High-Refractive-Index Substrates. *Org. Electron.* **2017**, *51*, 149-155.

[44] Tang, S.; Sandström, A.; Lundberg, P.; Lanz, T.; Larsen, C.; Reenen, S.; Kemerink, M.; Edman, L. Design Rules for Light-Emitting Electrochemical Cells Delivering Bright Luminance at 27.5 Percent External Quantum Efficiency. *Nat. Commun.* **2017**, *8*, 1190.

[45] Lu, J.-S.; Chen, H.-F.; Kuo, J.-C.; Sun, R.; Cheng, C.-Y.; Yeh, Y.-S.; Su, H.-C.; Wong, K.-T. Efficient Solid-State White Light-Emitting Electrochemical Cells Employing Embedded Red Color Conversion Layers. *J. Mater. Chem. C.* **2015**, *3*, 2802-2809.

[46] Su, H.-C.; Cheng, C.-Y. Recent Advances in Solid-State White Light-Emitting Electrochemical Cells. *Isr. J. Chem.* **2014**, *54*, 855-866.

[47] Su, H.-C. Optical Techniques for Light-Emitting Electrochemical Cells. *ChemPlusChem.* **2018**, *83*, 197-210.

[48] Yang, Z.-P.; Su, H.-C. Recent Advances in Optical Engineering of Light-Emitting Electrochemical Cells. *Adv. Funct. Mater.* submitted.

[49] Su, H.-C.; Chen, Y.-R.; Wong, K.-T. Recent Progress in White Light-Emitting Electrochemical

Cells. *Adv. Funct. Mater.* **2019**, 1906898.

[50] Hosseini, A. R.; Koh, C. Y.; Slinker, J. D.; Flores-Torres, S.; Abruña, H. D.; Malliaras, G. G. Addition of a Phosphorescent Dopant in Electroluminescent Devices from Ionic Transition Metal Complexes. *Chem. Mater.* **2005**, *17*, 6114-6116.

[51] Su, H.-C.; Lin, Y.-H.; Chang, C.-H.; Lin, H.-W.; Wu, C.-C.; Fang, F.-C.; Chen, H.-F.; Wong, K.-T. Solid-State Light-Emitting Electrochemical Cells Employing Phosphor-Sensitized Fluorescence. *J. Mater. Chem.* **2010**, *20*, 5521-5526.

[52] Chen, B.; Li, Y.; Chu, Y.; Zheng, A.; Feng, J.; Liu, Z.; Wu, H.; Yang, W. Highly Efficient Single-Layer Organic Light-Emitting Devices Using Cationic Iridium Complex as Host. *Org. Electron.* **2013**, *14*, 744-753.

[53] Tang, S.; Buchholz, H. A.; Edman, L. On the Selection of a Host Compound for Efficient Host-Guest Light-Emitting Electrochemical Cells. *J. Mater. Chem. C.* **2015**, *3*, 8114-8120.

[54] Lundberg, P.; Lindh, E. M.; Tang, S.; Edman, L. Toward Efficient and Metal-Free Emissive Devices: A Solution-Processed Host-Guest Light-Emitting Electrochemical Cell Featuring Thermally Activated Delayed Fluorescence. *ACS Appl. Mater. Interfaces.* **2017**, *9*, 28810-28816.

[55] Liu, J.; Oliva, J.; Tong, K.; Zhao, F.; Chen, D.; Pei, Q. Multi-Colored Light-Emitting Electrochemical Cells Based on Thermal Activated Delayed Fluorescence Host. *Sci. Rep.* **2017**, *7*, 1524.

[56] Moore, M. D.; Bowler, M. H.; Reynolds III, J. E.; Lynch, V. M.; Shen, Y.; Slinker, J. D.; Sessler, J. L. Ionic Organic Small Molecules as Hosts for Light-Emitting Electrochemical Cells. *ACS Appl. Mater. Interfaces.* **2018**, *10*, 24699-24707.

[57] Wu, M.-L.; Chen, G.-Y.; Shih, T.-A.; Lu, C.-W.; Su, H.-C. Effects of Tuning the Applied Voltage Pulse Periods on the Electroluminescence Spectra of Host-Guest White Light-Emitting Electrochemical Cells. *Phys. Chem. Chem. Phys.* **2018**, *20*, 18226-18232.

[58] Lenes, M.; Garcia-Belmonte, G.; Tordera, D.; Pertegás, A.; Bisquert, J.; Bolink, H. J. Operating Modes of Sandwiched Light-Emitting Electrochemical Cells. *Adv. Funct. Mater.* **2011**, *21*, 1581-1586.

[59] van Reenen, S.; Janssen, R. A. J.; Kemerink, M. Fundamental Tradeoff between Emission Intensity and Efficiency in Light-Emitting Electrochemical Cells. *Adv. Funct. Mater.* **2015**, *25*, 3066-3073.

[60] Kalyuzhny, G.; Buda, M.; McNeill, J.; Barbara, P.; Bard, A. J. Stability of Thin-Film Solid-State Electroluminescent Devices Based on Tris(2,2′-bipyridine)ruthenium(II) Complexes. *J. Am. Chem. Soc.* **2003**, *125*, 6272-6283.

[61] Sunesh, C. D.; Chandran, M.; Mathai, G.; Choe, Y. Highly Luminescent Yellow and Yellowish-Green Light-Emitting Electrochemical Cells based on Cationic Iridium Complexes with Phenanthroline based Ancillary Ligands. *Opt. Mater.* **2013**, *35*, 407-413.

[62] Optical simulation software: Setfos (FLUXiM), https://www.fluxim.com/.

[63] Wang, T.-W.; Su, H.-C. Extracting Evolution of Recombination Zone Position in Sandwiched Solid-State Light-Emitting Electrochemical Cells by Employing Microcavity Effect. *Org. Electron.* **2013**, *14*, 2269-2277.

[64] Jenatsch, S.; Regnat, M.; Hany, R.; Diethelm, M.; Nüesch, F.; Ruhstaller, B. Time-Dependent p-i-n Structure and Emission Zone in Sandwich-Type Light-Emitting Electrochemical Cells. *ACS Photonics* **2018**, *5*, 1591-1598.

[65] Naka, S.; Okada, H.; Onnagawa, H.; Tsutsui, T. High Electron Mobility in Bathophenanthroline. *Appl. Phys. Lett.* **2000**, *76*, 197-199.

[66] Meier, S. B.; van Reenen, S.; Lefevre, B.; Hartmann, D.; Bolink, H. J.; Winnacker, A.; Sarfert, W.; Kemerink, M. Dynamic Doping in Planar Ionic Transition Metal Complex-Based Light-Emitting Electrochemical Cells. *Adv. Funct. Mater.* **2013**, *23*, 3531-3538.